Clays and Clay Minerals, Vol. 35, No. 1, 29–37, 1987.

NONCRYSTALLINE Fe-Si-Al-OXYHYDROXIDES

RICHARD A. EGGLETON
Department of Geology, Australian National University
Canberra, ACT 2600, Australia

Abstract—High-resolution transmission electron microscopy of noncrystalline Fe-Si-Al-oxyhydroxide gels shows a common structure of hollow packed spheres having external diameters ranging from 50 to 1000 Å. Some sphere walls display a concentric structure, particularly if the gel composition is close to that of a crystalline clay mineral (e.g., smectite, kaolin). The spheres probably formed by expansion of void space (bubbles) as the surrounding gel contracted 5–10% because of partial ordering of the Fe-Si-Al-oxygen network. Much of the water contained in such noncrystalline minerals is incorporated within the bubbles.

Key Words—Gels, High-resolution transmission electron microscopy, Iron, Morphology, Noncrystalline oxyhydroxides.

INTRODUCTION

Noncrystalline materials are important constituents of soils and weathering profiles. It has long been recognized that many clay minerals crystallize from noncrystalline precursors, not only the paracrystalline allophane-imogolite clays formed in weathered volcanic deposits, but also those clays found in the saprolite formed on plutonic rocks. Even though their volume may not be great, such noncrystalline materials assume significance, because a considerable proportion of residual elements passes through this stage. Noncrystalline soil constituents have an added importance because of their extremely large surface area, making them particularly strong adsorbents of ions from solution (Parfitt, 1980); e.g., the high phosphorus content of some allophane (Webb and Finlayson, 1984).

The mineralogy of weathering is dominated by the three elements Si, Fe, and Al; at the stage of weathering of igneous rocks represented by loss of primary structure (end of saprolite stage), these three elements constitute 85% of the residual metals (Colman, 1982; Ildefonse, 1978). Consequently, most soil clay minerals can be classified on a triangular Fe-Si-Al diagram (Figure 1a); this classification is also convenient to describe noncrystalline minerals (Figure 1b). Compositions having Si:Al ratios between 1:1 and 1:2 have been extensively examined by Henmi and Wada (1976), Wada and Wada (1977), Kirkman (1977), Parfitt and Henmi (1980), and Tazaki (1982) in their investigations of allophane, imogolite, and the formation of halloysite. These workers have clearly demonstrated that allophane has a structure consisting of 50–70-Å diameter spheres, and that some allophane-like materials also show spherical structures. Much of the halloysite formed from volcanic ash and glass occurs in the form of spherical aggregates, and Eggleton and Buseck (1980) and Eggleton and Keller (1982) noted that spherical structures seem to be the precursors to smectite in the alteration of K-feldspar and limburgite glass.

In the course of examining the mechanism of mineral weathering, a number of reactions have been noted in which clay minerals form from noncrystalline material. Although in many samples the composition of the noncrystalline material is not accurately determinable, enough samples of analyzed bulk noncrystalline materials have been studied to allow some generalizations about their structure and their consequent crystallization to clay minerals. In this paper, transmission electron microscope results for noncrystalline materials in the Si <0.6 region of the Fe-Si-Al diagram are described, and a model is proposed for the crystallization of clay minerals from a noncrystalline or gel state.

METHOD

All minerals were examined by transmission electron microscopy (TEM) using JEOL 100CX and 200CX instruments. Samples were dispersed on holey carbon grids and initially photographed at low beam currents and magnification to check for changes in materials caused by beam damage. Such an initial examination is particularly important in studying noncrystalline materials, because one type of electron beam damage of crystalline framework silicates is the development of circular noncrystalline patches. As will be discussed below, spherical bodies are common in noncrystalline materials; those shown in this paper were present on first examination and either survived appreciable beam exposure, or degraded with exposure; hence they are not artifacts of observation.

Chemical data (Table 1) were obtained either by bulk analysis of homogeneous material or by energy-dispersive electron microprobe analysis. Neither technique can resolve chemical changes at the scale of the

Copyright © 1987, The Clay Minerals Society

https://doi.org/10.1346/CCMN.1987.0350104 Published online by Cambridge University Press

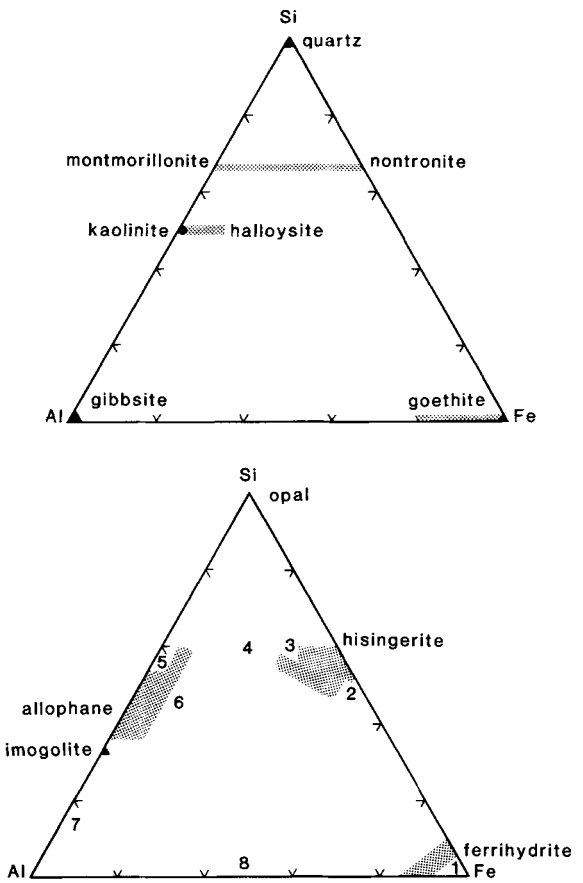


Figure 1. Triangular Si-Al-Fe composition diagrams of (a) common crystalline soil minerals, and (b) noncrystalline or poorly crystalline minerals. Numbers refer to compositions discussed in the text. Shading indicates compositional range.

objects observed (~100 Å); heterogeneous material was further qualitatively analyzed by scanning-transmission electron microscopy (STEM) at a resolution of about 200 Å.

SAMPLE DESCRIPTION AND RESULTS

Ferrihydrite ($Fe_{95}Si_5Al_0$)

Ferryhydrite is an iron oxyhydroxide of ideal composition $5Fe_2O_3 \cdot 9H_2O$. Natural ferrhydrites commonly contain silica and alumina and are so poorly crystalline that their X-ray powder diffraction (XRD) patterns may only show from two to six rather broad reflections (Chukhrov *et al.*, 1973). Samples were kindly provided by R. W. Fitzpatrick, CSIRO Division of Soils, Adelaide, South Australia; their composition is given in Table 1. About 94% of the Fe in sample 1a (Figure 1b) is ammonium oxalate (pH 3) extractable and inferred to occur as ferrihydrite; the remainder of the iron is in goethite. Quartz is present in this sample; STEM microanalysis indicates 5% SiO_2 in the ferrihydrite. Sample 1b is better crystallized than sample 1a, showing six broad XRD lines. About 76% of the Fe is ammonium oxalate extractable; the sample also contains quartz, goethite, and kaolinite.

Some of the TEM images from these samples (Figures 2a and 2b) show aggregates of spheres, many of which have margins which are more electron dense than the centers. Sphere diameters range from 50 to 100 Å, and the denser margins are 20–30 Å across. Other images (not shown) reveal aggregates of roughly spherical shape but without evidence for a more dense margin. Not all ferrihydrites show spherical structures such as is shown in Figure 2; in particular, synthetic ferrihydrites and some natural samples examined in this laboratory are aggregates of 60-Å diameter faceted crystals (unpublished results).

Hisingerite ($Fe_{46}Si_{52}Al_2$)

This sample of hisingerite (sample 2; Figure 1b) was described by Eggleton *et al.* (1983) as their sample S1. The TEM images they published are similar to those of ferrihydrite, showing 50- to 100-Å diameter spheres having walls as thick as 30 Å. No evidence of crystallinity was found in this sample, either by XRD or TEM lattice-image techniques.

Hisingerite ($Fe_{30}Si_{60}Al_{10}$)

Shayan (1984) described this hisingerite (sample 3; Figure 1b) from weathered basalt, and kindly provided a sample. The morphological features shown in Figure 3 largely reproduce those described by Shayan. Here also, the texture is dominated by spheres, ranging in size from 150 to 200 Å. The walls show marked contrast compared to the centers; many have concentric lattice fringes spaced at 3 Å, and some walls also show cross fringes spaced at 4.5 Å. Some straighter segments show 10-Å, 2:1 phyllosilicate layers, suggesting the presence of nontronite.

Limburgite glass ($Fe_{20}Si_{60}Al_{20}$)

The palagonitization of limburgite (sample 4; Figure 1b) was studied by Eggleton and Keller (1982) who showed that crystallization of smectite followed the development of spheres ranging in diameter from 200 to 600 Å.

Weathered plagioclase ($Fe_0Si_{50}Al_{50}$)

The weathering of basaltic plagioclase (sample 5; Figure 1b) is the subject of a current study in this laboratory. Microprobe analyses and STEM data indicate an alteration product having higher Al:Si ratio than the parent feldspar (labradorite, Si:Al = 2.5:1.5). Figure 4 shows spheres with high contrast walls adjacent to, and merging into, completely structureless material.

https://doi.org/10.1346/CCMN.1987.0350104 Published online by Cambridge University Press

Table 1. Chemical analysis.

	1a Dam Wall ferrihydrite	1b Palm Beach ferrihydrite	2 Hisingerite	3 Hisingerite	4 Glass	6 Cordierite	7 Allophane	8 Pisolite
SiO_2	17.72	18.34	35.19	32.40	45.7	46.60	10.97	1.02
TiO_2	0.21	0.40	—[3]	0.28	5.0	—	—	1.98
Al_2O_3	2.45	5.58	0.96	4.16	13.0	39.77	44.27	33.53
Fe_2O_3	59.41	61.34	37.84[2]	21.73[2]	17.20	0.95	0.44	46.84
MnO	0.07	0.02	3.72	0.04	—	—	—	—
MgO	0.50	0.20	0.11	5.19	5.1	0.52	0.35	0.24
CaO	1.71	0.23	0.19	0.68	1.8	0.47	—	—
Na_2O	0.31	0.05	—	0.67	0.50	0.43	0.37	—
K_2O	0.23	0.13	0.01	0.26	1.4	0.37	—	—
P_2O_5	1.18	0.01	0.25	0.00	n.d.[4]	n.d.	9.37	n.d.
H_2O	15.74	13.18	18.86	30.70	n.d.	n.d.	n.d.	n.d.
Total	99.53	99.50	98.33	96.11	89.7	89.02	65.77	83.61

1a. 'Dam Wall' ferrihydrite (R. W. Fitzpatrick, personal communication).
1b. Palm Beach ferrihydrite (R. W. Fitzpatrick, personal communication).
2. Hisingerite (sample S1, Eggleton *et al.,* 1983).
3. Hisingerite (Shayan, 1984).
4. Palagonitized glass (Eggleton and Keller, 1982).
6. Halloysite in weathered cordierite. Microprobe analysis.[1]
7. Allophane flow-stone (from Webb and Finlayson, 1984). Microprobe analysis.[1]
8. Laterite pisolite, most aluminous analysis. Microprobe analysis.[1]

[1] Technisch Physich Dienst energy dispersive electron microprobe, N. Ware, analyst.
[2] FeO in reported analysis recalculated as Fe_2O_3.
[3] — = below detection limit.
[4] n.d. = not determined.

The spheres range from 100 to 200 Å in diameter, and the walls appear to be thin (~20 Å), however, this material is prone to electron beam damage, and high-resolution photographs have not been possible to obtain.

Weathered cordierite ($Fe_{10}Si_{45}Al_{45}$)

Another study in this laboratory has shown cordierite (sample 6; Figure 1b) to transform to halloysite via a noncrystalline phase that has an estimated composition between that of the cordierite and the halloysite. The halloysite occurs as an array of packed 1000-Å diameter spheres, with concentric structures as small as 50 Å in diameter (Figure 5). Only *hk* diffraction data were obtained for this material; it has been called halloysite on the basis of its chemistry and spherical texture, which is comparable to that of many published TEM images of spherical halloysite (e.g., Tazaki, 1982; Sudo *et al.,* 1981).

Allophane ($Fe_1Si_{17}Al_{82}$)

Allophane has been the subject of much electron microscope research, and its structure consists of hollow, 50-Å diameter spheres. Wada (1982) restricted the term allophane to material having an Al:Si ratio between 0.5 and 1.0; materials containing less Si were referred to as 'allophane-like.' Webb and Finlayson (1984) described an allophane having a low Si:Al ratio and containing considerable phosphorus and carbon. Micrographs of material provided by these authors show some spheres ranging in size from 100 to 1000 Å (Figures 6a and 6b). Other areas are almost completely structureless (Figure 6c).

Lateritic pisolite ($Fe_{65}Si_0Al_{35}$)

Magnetic pisolites from a Tertiary laterite formed on basalt at Windellama, New South Wales, Australia, have a core rich in Al surrounded by a Al-poor rim (Figure 7a). XRD analysis shows the bulk of the pisolite to be noncrystalline with a small amount of maghemite. Bright- and dark-field TEM shows the maghemite crystals, about 200 Å in diameter, are scattered in a noncrystalline matrix (Figure 7b). The noncrystalline material contains Fe and Al only (STEM probe) in about a 2:1 proportion, comparable to the most Al-rich samples analyzed by electron microprobe. TEM images (Figures 7c and 7d) show evidence for spherical structures ranging from 20 to 200 Å, with an average diameter of 100 Å, and wall thickness of 10 to 50 Å. The thicker walls show a suggestion of a concentric structure having a 10-Å spacing.

DISCUSSION

Images from a range of natural Fe-Si-Al-oxyhydroxides show a similar texture of spherical aggregates regardless of composition. In each sample examined, the material appears to consist of bubbles or a foam of

https://doi.org/10.1346/CCMN.1987.0350104 Published online by Cambridge University Press

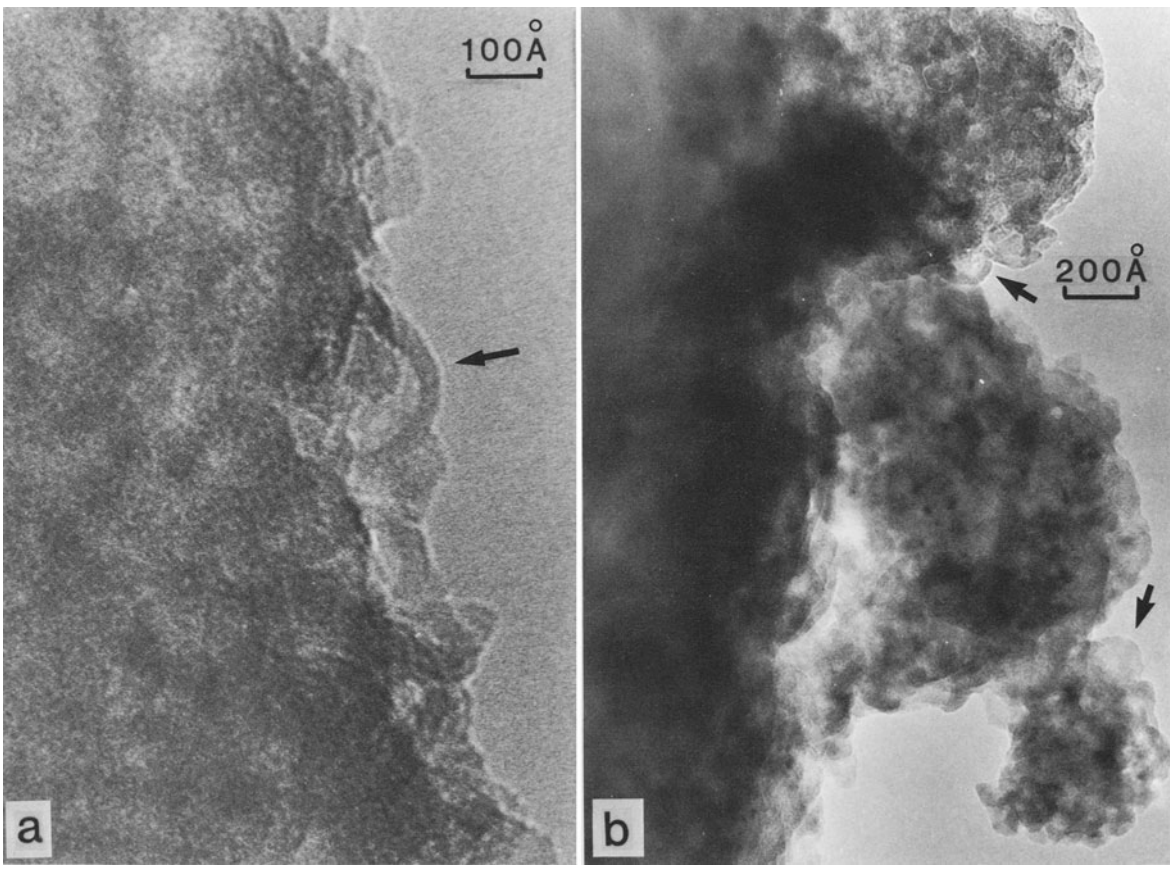


Figure 2. Transmission electron micrographs of (a) two-line ferrihydrite (sample 1a, Table 1) consisting of an aggregate of spheres having more electron-dense walls than centers; and (b) six-line ferrihydrite (sample 1b, Table 1). Arrows indicate spherical structures.

hydrous Fe-Al-silicate gel. Si and Al are commonly regarded as network formers in glasses (Henderson, 1982; Kirkpatrick, 1983); other cations are referred to as network modifiers. In these low-temperature forming materials, Fe^{3+} also appears to be a network former. A summary of the structure of tetrahedral oxide glasses (Phillips, 1982) concluded that they have spherical domains 60–100 Å in diameter; hence, noncrystalline Si-Al-Fe-oxide gels may be very similar to such glasses.

Theories of crystallization have evolved from studies of crystals forming in media permitting relatively rapid diffusion (see, e.g., Kirkpatrick, 1983). The formation of a nucleus of ordered material apparently reduces the bulk free energy of the system, but introduces a new surface (between crystal and medium), thereby increasing the total free energy and rendering the nucleus unstable. If a critical radius is reached, however, beyond which the surface energy term is overcome by the volume term, the nucleus grows (see, e.g., Henderson, 1982, p. 197).

Solid state crystallization introduces an additional factor, the strain energy developed when a more ordered (smaller volume) phase contracts from the disordered bulk, or when exsolution juxtaposes two phases of different dimension. The free energy change for nucleation (Henderson, 1982, p. 208) is $\Delta G = 4\pi r^2\sigma + 4/\pi r^3(\Delta G_v + \Delta G_s)/3$, where σ is the surface energy, r is the nucleus radius, ΔG_v is the free energy change/unit volume of the noncrystalline to crystalline state, and ΔG_s is the strain free energy. $\Delta G_v = -$ve, and $\Delta G_s = +$ve. In spinodal decomposition leading to exsolution and the formation of two discrete crystalline phases, ΔG_s is minimized because the two phases make contact along minimum strain surfaces. Spinodal decomposition involves the diffusion of a relatively mobile species through a largely fixed framework (e.g., K and Na diffusing through an aluminosilicate feldspar framework).

The TEM results presented here indicate that gel crystallization follows neither of these paths. No critical nucleus seems to form, nor does evidence exist for spinodal decomposition, particularly as in those examples where a crystalline phase ultimately results (halloysite, smectite, goethite), only a single composition is produced.

The bonding characteristics of an Fe-Si-Al oxide gel

https://doi.org/10.1346/CCMN.1987.0350104 Published online by Cambridge University Press

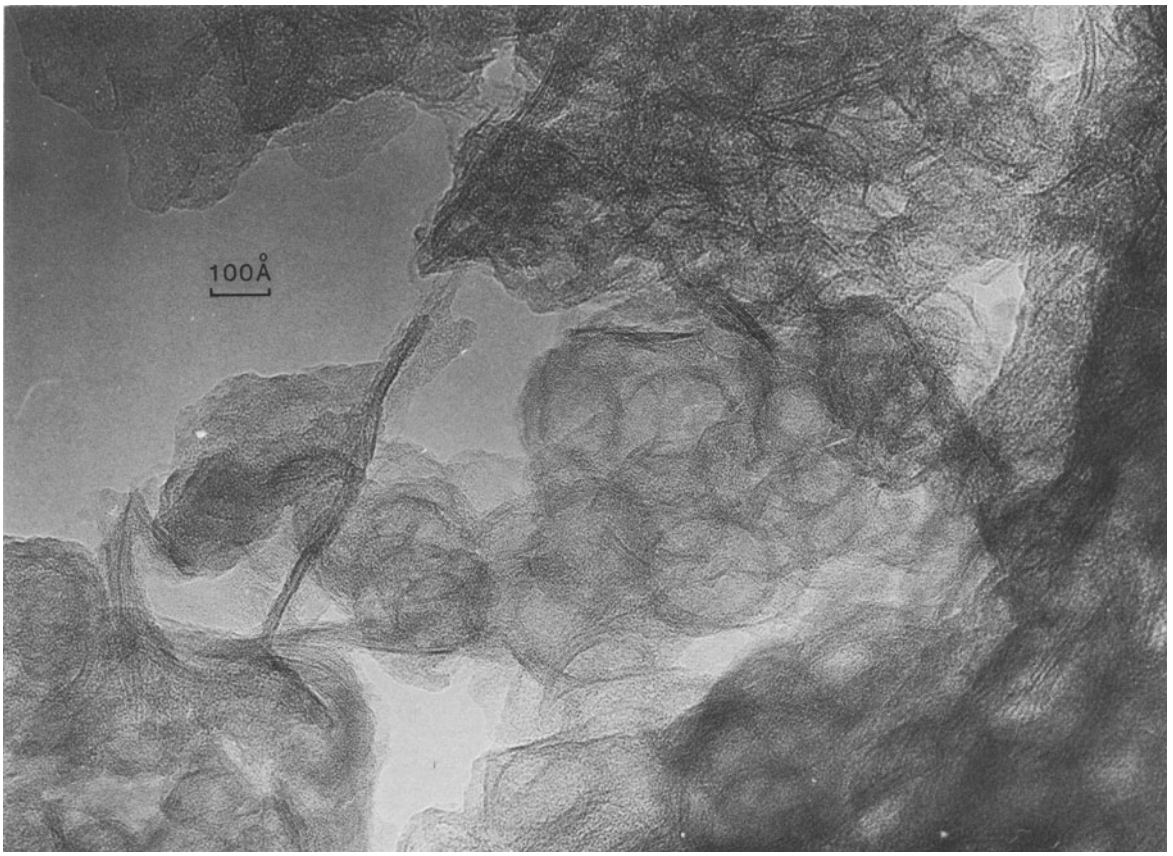


Figure 3. Transmission electron micrograph of hisingerite showing a structure dominated by packed hollow spheres. Some sphere walls show concentric 3-Å lattice fringes.

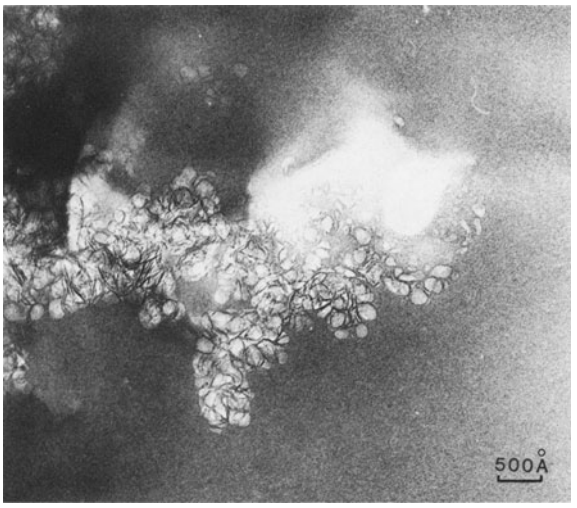


Figure 4. Transmission electron micrograph showing spherical structures formed from a noncrystalline precursor in weathered plagioclase.

are probably the same as those of crystalline materials of similar composition (Eitel, 1964). Assuming an uninterrupted network, the gel can be expected to be stronger than corresponding layer silicates, although the presence of water probably weakens a gel relative

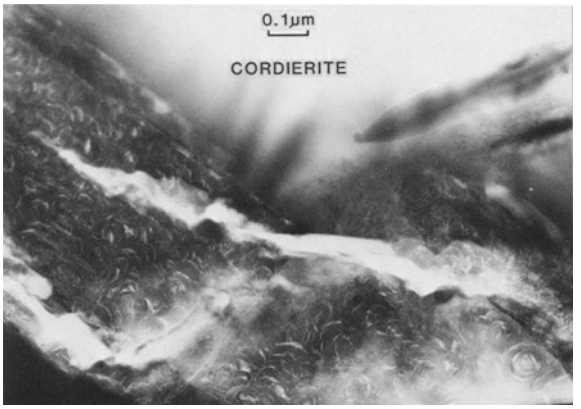
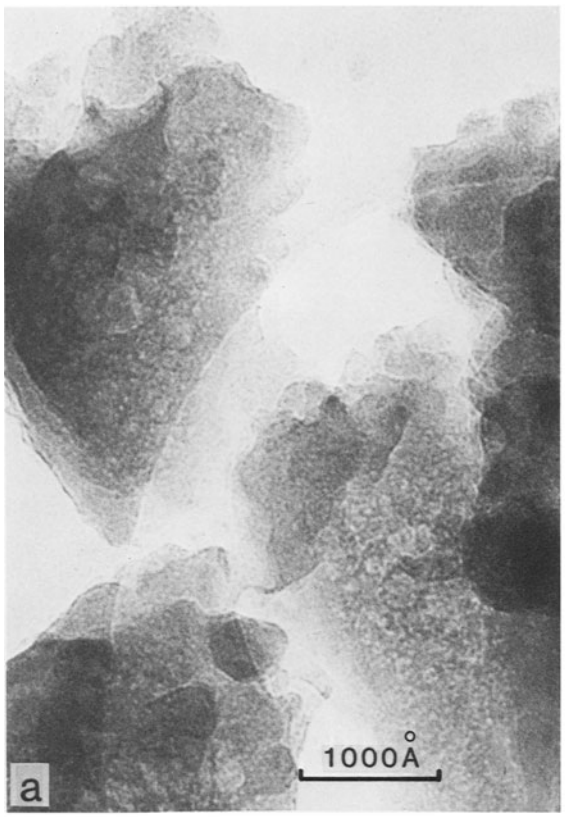
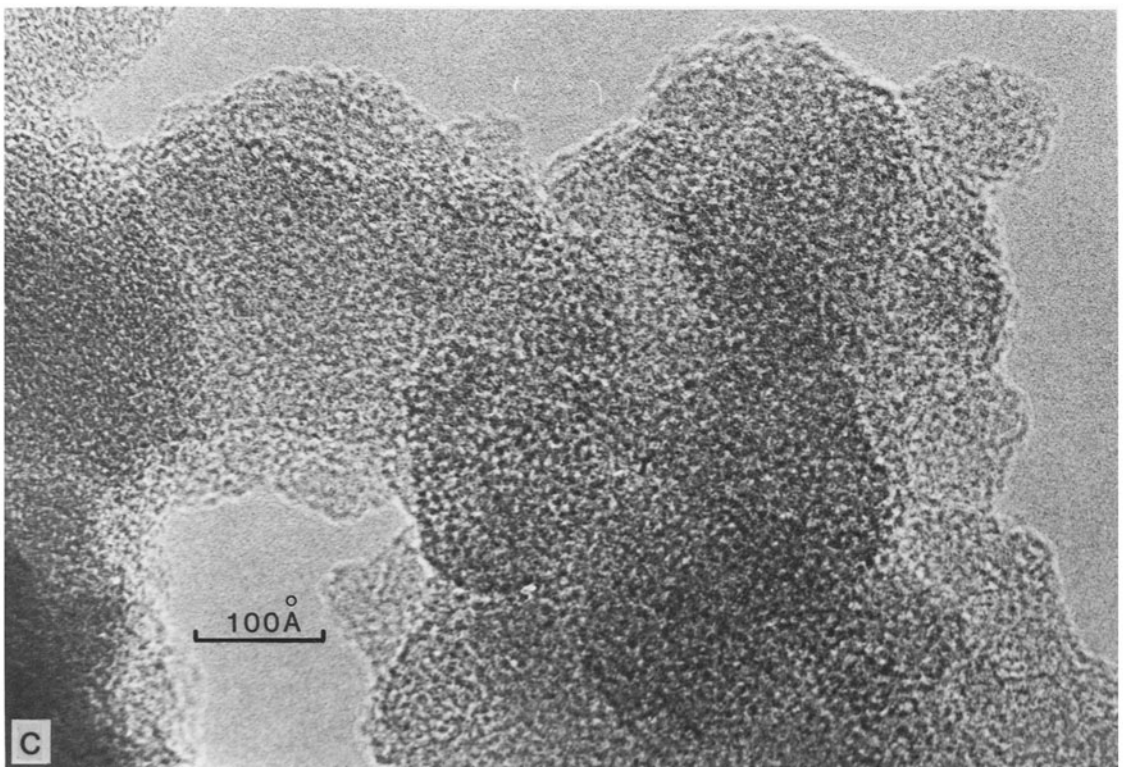


Figure 5. Transmission electron micrograph showing packed spheres of halloysite formed during the weathering of cordierite.

https://doi.org/10.1346/CCMN.1987.0350104 Published online by Cambridge University Press







https://doi.org/10.1346/CCMN.1987.0350104 Published online by Cambridge University Press

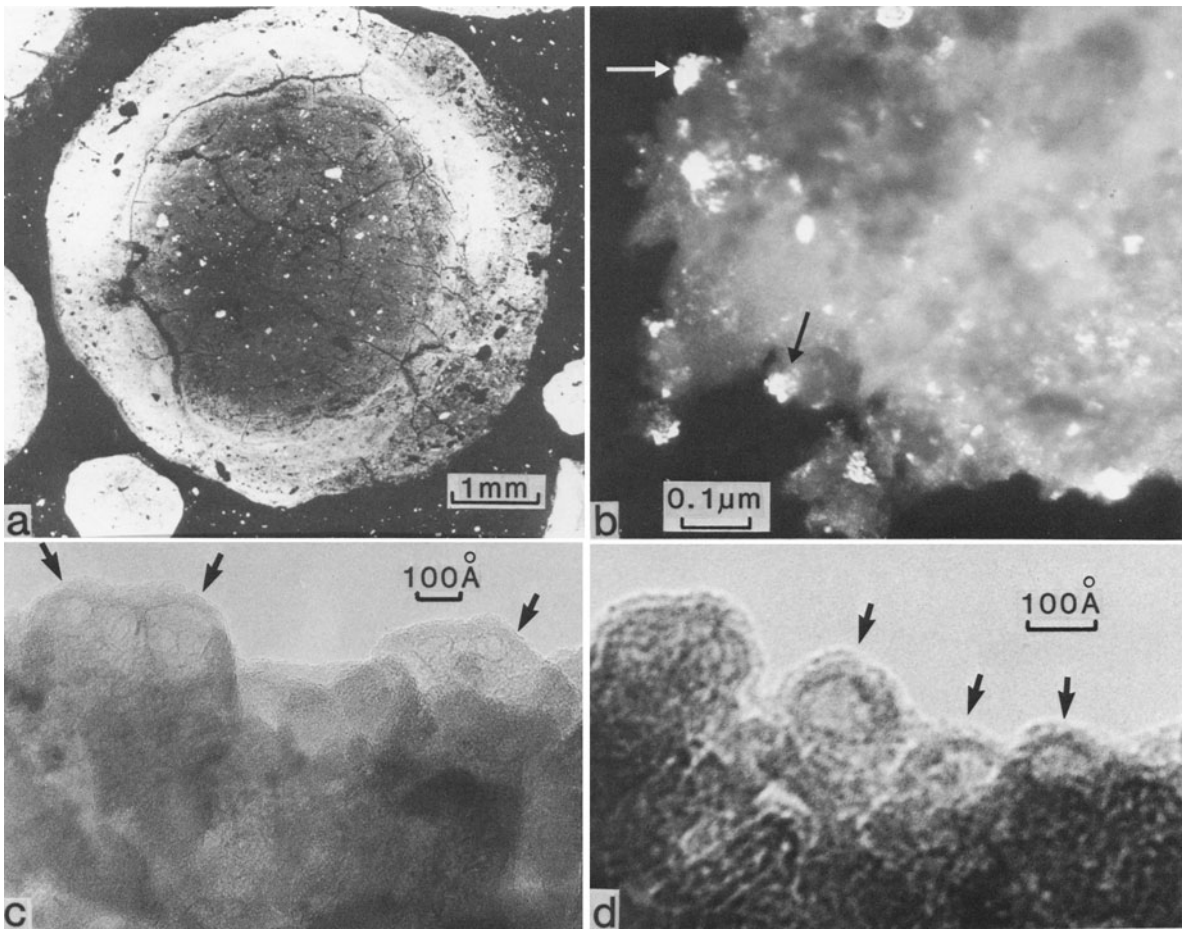


Figure 7. (a) Back-scattered electron image of lateritic pisolite. (b) Dark-field transmission electron micrograph showing maghemite (bright, arrowed) in a noncrystalline matrix. (c, d) Detail of matrix showing spherical structures (arrowed).

to a glass. Most of the samples examined here were too small or dispersed to allow their strength to be estimated; hisingerite has a Mohs hardness of 3; the allophane flow-stone sample has a hardness between 3 and 4. The free energy change in ordering from a glass to a crystal is of the order of 1% of the crystal free energy (about 40 kJ/mole), amounting to about 10^{-20} J per tetrahedral atom in silica or feldspars. Bond energy in silicates is 10 times this value (~400 kJ/g atom, Kirkpatrick, 1983), and calculations show that the complete crystallization of a 100-Å diameter sphere releases only enough energy to break a third of the bonds to the surrounding glass or gel. Thus, in the equation for the free energy change on nucleation, $|\Delta G_c| \geq |\Delta G_v|$ and nuclei are energetically forbidden.

Void nucleation

Although the nucleation of a crystal in a glass or gel is energetically unfavorable, the nucleation of a void appears to be energetically favorable. Void nucleation is envisaged as beginning at a point in the gel where contraction of the surrounding shell away from that point by partial ordering breaks a minimum of bonds between network-forming elements. For example, in a hexagonal network of tetrahedra, such as in tridymite, about one O–Si–O linkage exists per 20 Å^2. Thus, to nucleate a 100-Å diameter crystal by contraction involves the stretching or breaking of 750 bonds per sphere. To nucleate a void of 40-Å diameter in the same sphere volume involves at most 240 bonds. Nu-

←

Figure 6. Transmission electron micrographs of allophane-like materials showing (a, b) hollow spheres of various sizes and (c) structureless spherical domains.

https://doi.org/10.1346/CCMN.1987.0350104 Published online by Cambridge University Press

cleation of 40-Å voids at 100-Å intervals gives rise to the observed bubble pattern. A 100-Å sphere with a 40-Å diameter central void has a volume 6% less than that of the original 100-Å sphere of gel. The change in volume between silicate glasses and crystals (e.g., feldspar) is between 6% and 10%; thus, the observed holes in the spheres are of the correct size to be the result of contraction due to ordering.

Bubble-wall crystallization

Although most of the materials examined here were still largely noncrystalline, enough structure had developed in some bubble walls to suggest a further stage of crystallization. Evidence of a concentric or layer structure within the walls of hisingerite (sample 3), allophane (sample 7), and the laterite pisolite (sample 8) suggest the incipient development of crystallinity, for which the formation of octahedral and tetrahedral sheets in allophane (Wada and Wada, 1977) is a probable model. If a bubble wall eventually crystallizes to a clay mineral, the crystal thickness will be determined by the original sphere dimensions. For example, smectites 6 or 7 layers thick (a common thickness by XRD measurement) could result from the crystallization of the 60-Å wall between two spheres 100 Å apart.

Further crystallization may depend on the Si:(Al + Fe) ratio and on the existence of a clay mineral of appropriate composition. For example, the products of cordierite and feldspar weathering have Si:Al ratios close to 1:1, suitable for the formation of halloysite, and the volcanic glass (sample 4) has an Si:(Al + Fe) ratio close to 2:1, as do smectites (Mg makes up the difference in this sample). Hisingerite (sample 3) has a slight octahedral deficiency relative to smectite, and contains only a few crystallized 2:1 layers, generally in larger diameter spheres. Hisingerite (sample 2) has a Si:(Al + Fe) ratio close to 1:1, a composition for which no clay mineral is stable. This sample, like the allophane sample, shows little evidence of crystallinity. Evidently diffusion through these network gels is extremely difficult, even though they are hydrous. Most of the water shown in the analyses is probably held on the inside of the spheres, for a moderate positive correlation exists between the diameter of the larger voids and the water content (or difference from 100% for probe analyses), suggesting that much of the water is inside the bubbles.

From earlier studies of hisingerite-neotocite and limburgite glass Eggleton *et al.* (1983) and Eggleton and Keller (1982) postulated that bubble diameter exerted a control on the rate of crystallization of the bubble walls. A 2:1 layer silicate is normally planar, because the two tetrahedral sheets on either side of the octahedral sheet are of equal lateral dimensions, whereas 1:1 layer silicates may be curved as a result of inequality in the size of the component sheets (e.g., tubular halloysite, serpentine, Sudo *et al.*, 1981).

A 2:1 layer may be able to curve to some extent if the tetrahedral sheet on one side of the layer shrinks (by tetrahedral rotation); the minimum theoretical radius of curvature is about 120 Å (Eggleton and Keller, 1982). The crystallization of 1:1 halloysite with sphere diameters as small as 50 Å contrasts with the failure of the higher-silica hisingerite to form crystalline layer structures with curvatures of less than about 100-Å radius. Ferrihydrite also shows no concentric layer structure, presumably because the connected octahedral layers of the corundum structure type allow no curvature. Discussion of the allophane sample shown here is limited by the extra complication introduced by the presence of the network-forming phosphorus.

Bubble growth is not the only mechanism of clay mineral crystallization. The materials reported here are largely from relatively extensive volumes of gel (except samples 5 and 6), and, in the absence of other controls, bubble growth may have been the common process. Other mechanisms, however, such as epitactic and topotactic growth, appear to dominate when clays form oriented aggregates that pseudomorph earlier formed crystals. Inherited short segments of structural sequences (e.g., perhaps, amphibole chains, Banfield, 1985) may also provide the nuclei on which layer silicates grow.

SUMMARY

Noncrystalline Fe-Si-Al-oxyhydroxides commonly show a structure of packed hollow spheres, similar to a bubble foam. The spheres range in diameter from 50 to 1000 Å, but are commonly 100–200 Å across. Bubble walls may show an incipient layer structure that develops into crystalline layer silicates if the gel has a smectite or kaolinite composition.

This structure probably forms after shrinkage caused by the partial ordering of the noncrystalline gel. Contraction of the gel away from the point of an initial weakness produces a void which enlarges as the bubble wall crystallizes further. A volume reduction of 6% is apparently enough to produce the observed 40-Å voids in 100-Å diameter spheres.

ACKNOWLEDGMENTS

I am grateful to B. G. Hyde and the Research School of Chemistry for access to the electron microscopes, and to A. Shayan, J. A. Webb, and R. W. Fitzpatrick for samples. G. Sellar photographed the ferrihydrite.

REFERENCES

Banfield, J. F. (1985) Mineralogy and chemistry of granite weathering: M.Sc. thesis, Australian National University, Australia, 229 pp.

https://doi.org/10.1346/CCMN.1987.0350104 Published online by Cambridge University Press

Chukhrov, F. W., Zvyagin, B. B., Ermilova, L. P., and Gorshkov, A. I. (1973) New data on iron oxides in the weathering zone: in *Proc. Int. Clay Conf., Madrid, 1972,* J. M. Serratosa, ed., Div. Ciencas C.S.I.C., Madrid, 333–341.

Colman, S. M. (1982) Chemical weathering of basalts and andesites: Evidence from weathering rinds: *U.S. Geol. Surv. Prof. Pap.* **1246,** 51 pp.

Eggleton, R. A. and Buseck, D. R. (1980) High-resolution electron microscopy of feldspar weathering: *Clays & Clay Minerals* **28,** 173–178.

Eggleton, R. A. and Keller, J. (1982) The palagonitisation of limburgite glass—a TEM study: *N. Jb. Miner. Mh. Jg.* **1982,** 321–336.

Eggleton, R. A., Pennington, T. H., Freeman, R. S., and Threadgold, I. M. (1983) Structural aspects of the hisingerite–neotocite series: *Clay Miner.* **18,** 21–31.

Eitel, W. (1964) *Silicate Science VI: Silicate Structures:* Academic Press, New York, 666 pp.

Henderson, P. (1982) *Inorganic Geochemistry:* Pergamon Press, New York, 353 pp.

Henmi, T. and Wada, K. (1976) Morphology and composition of allophane: *Amer. Mineral.* **61,** 379–390.

Ildefonse, P. (1978) Mécanismes de l'altération d'une roche gabbroïque du Massif du Pallet (Loire Atlantique): Doctorat Thèse, Université de Poitiers, Poitiers, France, 142 pp.

Kirkman, J. H. (1977) Possible structure of halloysite disks and cylinders observed in some New Zealand rhyolitic tephras: *Clay Miner.* **12,** 199–216.

Kirkpatrick, R. J. (1983) Theory of nucleation in silicate melts: *Amer. Mineral.* **68,** 66–67.

Parfitt, R. L. (1980) Chemical properties of variably charged soils: in *Soils with Variable Charge,* B. K. G. Theng, ed., Soil Bureau D.S.I.R., Lower Hutt, New Zealand, 167–194.

Parfitt, R. L. and Henmi, T. (1980) Structure of some allophanes from New Zealand: *Clays & Clay Minerals* **28,** 285–294.

Phillips, J. C. (1982) Spectroscopic and morphological structure of tetrahedral oxide glasses: *Solid State Physics* **37,** 93 pp.

Shayan, A. (1984) Hisingerite material from a basalt quarry near Geelong, Victoria, Australia: *Clays & Clay Minerals* **32,** 272–278.

Sudo, T., Shimoda, S., Yotsumoto, H., and Aita, S. (1981) *Electron Micrographs of Clay Minerals:* Elsevier, Amsterdam, 203 pp.

Tazaki, K. (1982) Analytical electron microscopical studies of halloysite formation processes—morphology and composition of halloysite: in *Proc. Int. Clay Conf., Bologna, Pavia, 1981,* H. van Olphen and F. Veniale, eds., Elsevier, Amsterdam, 573–584.

Wada, K. (1982) Amorphous/clay minerals—chemical composition, crystalline state, synthesis, and surface properties: in *Proc. Int. Clay Conf., Bologna, Pavia, 1981,* H. van Olphen and F. Veniale, eds., Elsevier, Amsterdam, 385–398.

Wada, S.-I. and Wada, K. (1977) Density and structure of allophane: *Clay Miner.* **12,** p. 289.

Webb, J. A. and Finlayson, B. L. (1984) Allophane and opal speleothems from granite caves in southeast Queensland: *Aust. J. Earth Sci.* **31,** 341–349.

(Received 15 February 1986; accepted 3 September 1986; Ms. 1559)

https://doi.org/10.1346/CCMN.1987.0350104 Published online by Cambridge University Press